

Retinal Blood Vessels Segmentation Using the Radial Projection and Supervised Classification

Qinmu Peng¹, Xinge You^{1,2}, Long Zhou², Yiu-ming Cheung³

¹Department of Electronics and Information Engineering,
Huazhong University of Science and Technology, Wuhan, China

Email: pqinmu@gmail.com youxg@mail.hust.edu.cn

²Department of Electrical and Information Engineering,
Wuhan Polytechnic University, Wuhan, China

Email: profzh@126.com

³Department of Computer Science, Hong Kong Baptist University, Hong Kong

Email: ymc@comp.hkbu.edu.hk

Abstract

The low-contrast and narrow blood vessels in retinal images are difficult to be extracted but useful in revealing certain systemic disease. Motivated by the goals of improving detection of such vessels, we propose the radial projection method to locate the vessel centerlines. Then the supervised classification is used for extracting the major structures of vessels. The final segmentation is obtained by the union of the two types of vessels after removal schemes. Our approach is tested on the STARE database, the results demonstrate that our algorithm can yield better segmentation.

1. Introduction

Retinal images provide considerable information on pathological changes caused by local ocular disease which reveals diabetes, hypertension, arteriosclerosis, cardiovascular disease and stroke [1]. Computer-aided analysis of retinal image plays a central role in diagnostic procedures. However, automatic retinal segmentation is complicated by the fact that retinal images are often noisy, poorly contrasted, and the vessel widths can vary from very large to very small.

Considerable previous works have endeavored to address these issues. The matched filter and the adaptive threshold methods have been tried in [2, 3, 4]; and the classification methods [5, 6, 7] are used. Tracking-based method [8] also provides a satisfactory description of the vessel network. The existing methods make greatly progress in the vessel segmentation, including

the SVM [7] and FLUX [9], which are also devoted to the segmentation.

2. Locating the vessel centerlines using radial projection

It has been observed that blood vessels in retinal images have nice properties which are valuable for mathematic modeling. The blood vessels usually have small curvatures, they are piecewise linear and gradually change in intensity along their lengths.

We shall give the mathematical description for the radial projection. In the spatial domain, $f(x, y)$ represents an image, (x, y) is associated with a pixel location. First, $f(x, y)$ in the Cartesian coordinates is transformed into the polar coordinates:

$$\begin{cases} x = \gamma \cos \theta \\ y = \gamma \sin \theta \end{cases} \quad (1)$$

Hence,

$$p(x, y) = p(\gamma \cos \theta, \gamma \sin \theta) \quad (2)$$

Where γ is the radius of projection, θ is the radial direction, and $p(x, y)$ is the intensity of a pixel at (x, y) . For any fixed θ , we compute the following summation:

$$f(\theta) = \sum_{\gamma=0}^{\gamma} p(\gamma \cos \theta, \gamma \sin \theta) \quad (3)$$

The resulting $f(\theta)$ is in fact equal to the total pixels as distributed along the radial direction θ , also is the VRP (VRP means the value of radial projection for a

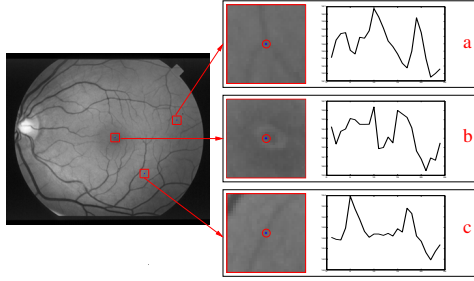


Figure 1. Illustration of a given pixel (blue color) in three typical regions and the corresponding projected curves.

pixel at a specific orientation) in the projected curve at the θ . Obviously, the value of $f(\theta)$ increases significantly if this direction is aligned within a vessel. We set $N = 24$, so we obtain an angular resolution of 15° to span all possible directions. This resolution is satisfactory with respect to the radius of projection, also a acceptable tradeoff between computational cost and detection performance.

Each pixel in the regions of interest (ROI) is taken as the center of radial projection; then, the projection is performed along different radial directions covering the whole circular region. Thus, the projected curve of each pixel consists of 24 VRP. The key idea is that the projected curve of a pixel usually has prominent peaks if the pixel belongs to a vessel segment. We exploit this fact and look for the prominent peaks by comparison with multi-adjacency values in the curve. Fig.1 illustrates three typical positions (linear segment, branching segment and noisy non-vessel regions) where a pixel usually is located. If the projected curve of a pixel displays prominent twin-peaks, the pixel has high possibility of belonging to a linear vessel segment, see Fig.1(c). Further, if the pixel is located in the vessel branching, its projected curve may show three or more prominent peaks, see Fig.1(a). Otherwise, the pixel may demonstrates disordered projected curve which is shown in Fig.1(b). Although some non-vessel pixels' curves may reveal the same curve shape like that of a vessel pixel, our removal scheme can largely clear these false pixels out.

To illustrate this process, an example for an image region containing a tree-like vessel with a narrow branch is shown in Fig. 2(a). The initial location of the most likely vessel centerlines are presented in Fig. 2 (b). The pruning operation is then carried out to remove the spuriously detected vessel pixels according to intensity of the pixel and length of the segment. Each candidate point is confirmed or rejected as a valid one based on

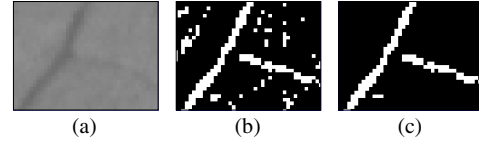


Figure 2. Locating the candidate centerline points. (a) Fragment of the inverted green channel of retinal image. (b) The image with centerline candidates after radial projection. (c) The image with centerline candidates are pruned according to intensity of the pixel and length of the segment.

these two features.

Firstly, we compute the median value in eight-connected neighborhood, the intensity of the candidate should be greater than the median value so as to pass the first artifact removal scheme.

Secondly, the length of the candidate pixel set is measured by counting the candidate pixels along the 24 orientations within eight pixels length, retaining the maximum directional counts as the length of the local segment, so the perfect vessel segment has eight pixels. In this removal step, if the length of any segment is smaller than $\ell = 5$, it should be removed. Here, ℓ is a user-defined threshold. This process is repeated and most of noisy pixels can be cleared out in Fig. 2 (c).

After the removal stage, most of the spurious objects are pruned. This de-noising strategy effectively protect the low contrast vessel pixels from clearing out compared to the conventional connected region method, because it allows for isolated vessel pixels near the vessel segment in addition to the local connectivity.

3. Extraction of the major structures of vessels

The supervised method [5],[7] is able to capture the major structures of vessels and produces good results near blood vessel edges, but it has limitations for the thinnest vessels that has been solved by the radial projection. In this part, supervised method is applied to obtain the major vessels. Each pixel is represented by a feature vector including line strength at different scales from the steerable complex wavelet transform. The resulting feature space is used to classify each pixel as either a vessel or non-vessel pixel using a support vector machine (SVM) classifier. A more detailed description for the approach will be provided.

1) *Steerable Complex Wavelet Transform*: Steerable filters provide a efficient way to compute the response of an oriented filter in an arbitrary orientation using a

finite number of basis filters with different orientations by Freeman and Adelson [10]. To seek a construction whose orientation selectivity is specified independently of radial frequency (or scale) selectivity, a steerable complex wavelet construction was developed by Bharath [11]. It has the ability to independently study orientation and scale selection paradigms.

For convenience in tuning angular and radial characteristics of the filters, Bharath imposed domain polar separability, so that an analysis filter $G_{0,k}(\omega, \phi)$ in the k th direction in a filter set can be specified as the product of a radial frequency function $\Omega_0(\omega)$ and angular frequency function $\Phi_{0,k}(\phi)$, i.e., $G_{0,k}(\omega, \phi) = \Omega_0(\omega)\Phi_{0,k}(\phi)$. More details can be found in [11]. The radial frequency function $\Omega_0(\omega)$ is based on Erlang functions which are one-sided density functions. We chose the Quadratic B-spline instead of Erlang functions in this work due to its smooth and compactly supported properties. It illustrates better directional selectiveness capability of detecting oriented features. The radial frequency functions are generated by the scale and translation of the Quadratic B-spline. It is defined as

$$\Omega_0 = \theta\left(\frac{\omega - \omega_0}{S(\omega_0)}\right) \quad (4)$$

Where $\theta(\cdot)$ is the Quadratic B-spline, and the ω_0 is frequency-shifting factor which indicates the center frequency of the bandpass filter. In retinal images, the vessels have various widths, we simply define the $\omega_0 = 1/\text{width}$ which is proportional to the vessel width. Denote $S(\omega_0)$ as scale function, i.e., $S(\omega_0) = \sqrt{2 \ln(2) \omega_0} / 2$. We use the same angular frequency characteristic in [11]:

$$\Phi_0(\phi) = \cos^3(\phi) \text{rect}(\phi/\pi) \quad (5)$$

Where $\text{rect}(\phi) = U(\phi + (1/2))U((1/2) - \phi)$ and $U(\cdot)$ is the unit step function. So the analysis filter $G_{0,k}(\omega, \phi)$ can be formed by the radial frequency function and angular frequency function. We apply the improved steerable filters to adaptively enhance the oriented vessels at different scales (the different vessel width), the corresponding center frequency ω_0 is $1, 1/2, 1/3, 1/5, 1/7$. So five enhanced retinal images with different scales can be obtained using the steerable complex wavelet transform.

2) *Feature Selection and Classification*: The line strength of the pixel [7] is a good feature to discriminate vessel pixels from the non-vessel pixels. Then based on the above five enhanced retinal images S and the original image $I(i, j)$, we construct the feature vector $\mathbf{x} = [S_1(i, j), S_2(i, j), \dots, S_5(i, j), I(i, j)]$, used to train a supervised classifier. The feature vector needs to be normalized which helps to compensate for intrinsic

Method	Accuracy	sensitivity	specificity
Hoover	0.9267	0.6751	0.9567
Soares	0.9480	0.7103	0.9737
Mendonça	0.9440	0.6996	0.9730
Proposed	0.9492	0.7256	0.9750
Second observer	0.9354	0.8949	0.9390

Table 1. Performance of vessel segmentation methods.

variation between images. Training is performed using 20 000 manually segmented pixels randomly extracted from the 20 images (500 vessel pixels and 500 non-vessel pixels per image), yielding the SVM classifier.

4. Union of the vessel centerlines and the major structures of vessels

We obtain the final segmentation vessels of retinal image by combining the vessel centerlines image with the major structures of vessels image which are derived from the above phases.

First, we roughly compute the width, length and the area of each vessel segment. Second, if any vessel segment in the major structures images is not near to any vessel centerlines and its width, length as well as area can't meet a user defined threshold, it will be removed. Then, the morphological "bridge" operation is performed on the image. This operation bridges unconnected pixels, that is, sets 0-valued pixels to 1 if they have two nonzero neighbors that are not connected. Finally, the pixels nearly surrounded by vessel points but not labeled as part of a vessel are considered, they are taken back using the four neighborhood connectivity. The complete vessel segmentation is obtained by performing a logical "or" operation on the vessel centerlines image and the denoised major structures of vessels image.

5. Experiments and results

The method described in the previous sections is evaluated on the STARE database. Performance is computed with the segmentations of the first observer as ground truth.

To facilitate the comparison with other retinal vessel segmentation approaches, the performances are evaluated using three different measures. In Table 1, our approach are compared with the most recent methods in terms of accuracy, sensitivity and specificity. The pro-

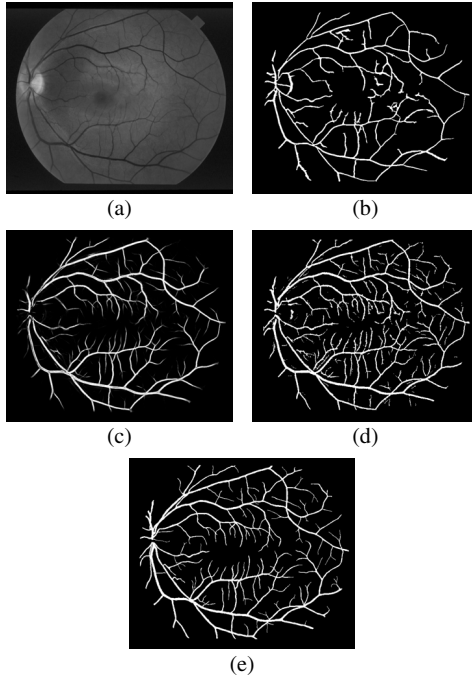


Figure 3. Results of a retinal image using different methods. (a) Retinal image (Im0255). (b) Hoover et al. method. (c) Soares et al. method. (d) Proposed method. (e) Ground truth 1.

posed algorithm gives higher average sensitivity rate in the same range of specificity and accuracy.

Fig. 3(b)-(d) show an example of results using different methods. Fig. 3(b) contains a few narrow vessels while Fig. 3(c) has more small ones. This is because a training image set is used in the latter method. The result of the proposed method is shown in Fig. 3(d), which is very close to the manual segmentation. We can see that the proposed method is able to detect many narrow and low-contrast vessels without producing many spurious spots. However, if there are more thread-like objects near the wide vessels, artifacts still can be formed.

6. Conclusions and discussions

In this paper we combine the radial projection and the supervised method to yield vessel segmentation. We detect the narrow vessels with low contrast based on the radial projection which is performed by the sum of a series of intensity of pixels along different radial directions. Thus, this operation can distinguish between vessel points and the background points, allowing the narrow vessel to stand out from the background. And the supervised method is applied to obtain the major struc-

tures of vessels, because it learns from human-labeled data, so it is able to extract better major vessels and decrease the false detection.

Acknowledgment

This work was supported by the grant 607731871 and 60973154 from the NSFC, NCET-07-0338 from the Ministry of Education, China. This work was also partially supported by a grant from the Research Grant Council of Hong Kong SAR under Project HKBU 210309 and by the Faculty Research Grant of Hong Kong Baptist University under Project: FRG2/0809/122.

References

- [1] A. M. Mendonça and A. Campilho. Segmentation of retinal blood vessels by combining the detection of centerlines and morphological reconstruction. *IEEE Trans. Med. Imag.*, 25(9):1200–1213, 2006.
- [2] S. Chauduri, S. Chatterjee, N. Katz, M. Nelson, and M. Goldbaum. Detection of blood vessels in retinal images using two-dimensional matched filters. *IEEE Trans. Med. Imag.*, 8(3):263–269, 1989.
- [3] A. Hoover, V. Kouznetsova, and M. Goldbaum. Locating blood vessels in retinal images by piecewise threshold probing of a matched filter response. *IEEE Trans. Med. Imag.*, 19(3):203–210, 2000.
- [4] X. Jiang and D. Mojon. Adaptive local thresholding by verification-based multithreshold probing with application to vessel detection in retinal images. *IEEE Trans. Pattern Anal. Mach. Intell.*, 25(1):131–137, 2003.
- [5] J. V. B. Soares, J. J. G. Leandro, R. M. C. Jr., H. F. Jelinek, and M. J. Cree. Retinal vessel segmentation using the 2d gabor wavelet and supervised classification. *IEEE Trans. Med. Imag.*, 25(9):1214–1222, 2006.
- [6] J. J. Staal, M. D. Abramoff, M. Niemeijer, M. A. Viergever, and B. van Ginneken. Ridge based vessel segmentation in color images of the retina. *IEEE Trans. Med. Imag.*, 23(4):501–509, 2004.
- [7] E. Ricci and R. Perfetti. Retinal blood vessel segmentation using line operators and support vector classification. *IEEE Trans. Med. Imag.*, 26(10):1357–1365, 2007.
- [8] Y. A. Tolia and S. M. Panas. A fuzzy vessel tracking algorithm for retinal images based on fuzzy clustering. *IEEE Trans. Med. Imag.*, 17(2):263–273, 1998.
- [9] A. Vasilevskiy and K. Siddiqi. Flux maximizing geometric flows. *IEEE Trans. Pattern Anal. Mach. Intell.*, 24(12):1565–1578, 2002.
- [10] W. T. Freeman and E. H. Adelson. The design and use of steerable filters. *IEEE Trans. Pattern Anal. Mach. Intell.*, 13(9):891–906, 1991.
- [11] A. A. Bharath and J. Ng. A steerable complex wavelet construction and its application to image denoising. *IEEE Trans. Image Process.*, 14(7):948–959, 2005.